Polymer Journal (2013) 45, 468–480

www.nature.com/pj

REVIEW

Self-assembled monolayers formed by helical peptide building blocks: a new tool for bioinspired nanotechnology

Emanuela Gatto and Mariano Venanzi

In this contribution, we report on our studies on peptide-based self-assembled monolayers (SAMs). In particular, we show that helical oligopeptides formed by C^{α}-tetrasubstituted amino acids and functionalized at the N terminus by a lipoic acid can form stable and densely packed nanometric films on a gold surface. The morphology of the peptide SAM was characterized by ultra-high-vacuum scanning tunneling microscopy and spectroscopic techniques, whereas their electronic conductivity was investigated by cyclic voltammetry and chronoamperometry in peptides functionalized with electroactive probes and by photocurrent generation experiments on peptides functionalized with photoactive groups. The versatility of helical peptide building blocks in the engineering of complex nanostructures is highlighted by the formation of multicomponent SAMs with a 'soft' approach based on the setting up of weak intermolecular interactions.
Polymer Journal (2013) **45,** 468–480; doi:10.1038/pj.2013.27; published online 27 March 2013

Keywords: conformationally constrained peptides; electron transfer; peptide self-assembled monolayers; SAM morphology

INTRODUCTION

Self-assembly, that is, the spontaneous organization of molecular building blocks to generate a supramolecular architecture, is the most promising approach for the construction of controlled nanometric structures.[1–3] This strategy has been leading to important achievements in several fields, providing new concept, smart materials for tissue engineering, controlled drug release, nucleic acid and protein sensing, organic photovoltaics and molecular electronics.[4–6]

Among the supramolecular architectures obtained by self-assembly (*bottom-up approach*), self-assembled monolayers (SAMs) have been demonstrated as the most suitable tool for modifying the surface properties of inorganic compounds (metals, semiconductors, polymers), paving the way for the realization of hybrid devices (*soft meets hard*).[2,7,8]

There are several reasons for investigating peptide-based SAMs. (i) *Peptides can be easily functionalized.* Chemists are currently able to synthesize amino acids endowed with specific functions and showing well-defined three-dimensional structural properties.[9] (ii) *The secondary structure adopted by the peptide backbone can be strictly controlled.* The careful selection of amino-acid residues allows one to design ordered secondary structures, such as 3_{10}- and α-helical segments, β-strands and β-hairpin motifs.[10] (iii) *Peptides show unique self-assembly properties*, giving rise to the formation of nano- and mesoscopic supramolecular architectures.[11] In the most popular alkanethiol SAMs, the ordering of the monolayer is driven by the strong Au/sulfur affinity (positional order) and the lateral van der Waals interaction between the tethered alkyl chains (orientational order).[12] Peptides expand the catalog of molecular interactions that stabilize self-assembled structures (interchain N–H $\cdots$ O = C hydrogen bonds, cysteine–cysteine disulfide bridges, interchain dipole interactions, stacking interactions between aromatic moieties). (iv) *The peptide bond is polar* (3.6 D per residue), so that, when the peptide chain folds in a helical structure, for example, α- or 3_{10}-helical conformation, the peptide dipole moments sum up to generate an electric macrodipole stabilized by head-to-tail interactions. It has been shown that the associated electrostatic field promotes directional electron transfer (ET) over long distances, giving rise almost exclusively to the charge-separated state stabilized by the electric macrodipole.[13,14]

Stable peptide SAMs on gold surfaces have been obtained by functionalizing the peptide chain with a thiol,[15] a disulfide group[16] or the thiol side chain of cysteine.[17] Lipoic acid has been also successfully employed to endow oligo- and polypeptides with a disulfide functionality at the N terminus.[18] This synthetic strategy promotes the linkage of a helical peptide to a gold surface, because the helix dipole, the positive end of which is located at the N terminus, has been shown to further stabilize the gold–sulfur interaction, conferring to the gold–sulfur bond a polar character (Au^{+}–S^{-}).[19] In this case, the peptide SAM gives rise to a negative surface potential, in contrast to the positive surface potential generated by alkanethiol monolayers.[20] Our recent work that we review in this contribution, has been focused on the use of conformationally constrained

Department of Chemical Sciences and Technologies, University of Rome Tor Vergata, Rome, Italy
Correspondence: Professor M Venanzi, Department of Chemical Sciences and Technologies, University of Rome Tor Vergata, Via Ricerca Scientifica 1, Rome 00133, Italy.
E-mail: venanzi@uniroma2.it
Received 6 November 2012; revised 24 January 2013; accepted 25 January 2013; published online 27 March 2013

oligopeptides as building blocks of SAMs chemisorbed on gold surfaces. Specifically, the use of C^{α}-tetrasubstituted amino acids allowed us to obtain rigid helical oligopeptides able to form densely packed SAMs. This approach is particularly suitable in relation to electronic and sensing applications for two reasons: (i) the exponential fall off of the ET efficiency, and hence of the intensity of the electrochemical signal, with the thickness of the peptide film and (ii) the unique electronic conduction properties of helical peptides, the high efficiency of which is determined by two competitive mechanisms: tunneling (superexchange (SE)) through the peptide bridge (predominant for short distances) and electron hopping through the amide sites. The latter mechanism has been shown to allow for long-range ET over nanometric distances.[21]

In the first part of the paper, we will describe the morphology of peptide SAMs formed by helical oligopeptides and the dynamic character of their building up, whereas in the second part, we will resume our results on their ground- and excited-state ET properties by electrochemical and photoinduced current generation experiments, respectively. In the end, we will show our recent results on the engineering of multicomponent peptide SAMs by a 'soft' approach based on the exploitation of weak intermolecular interactions. The amino-acid sequences and the acronyms adopted along the text for the peptide building blocks forming the SAMs described in this review are reported in Figure 1.

MORPHOLOGY OF SAMS FORMED BY CONFORMATIONALLY CONSTRAINED OLIGOPEPTIDES

The first peptide system investigated by us was an hexapeptide formed by five α-aminoisobutyric acid (Aib) residues and a tryptophan (Trp) unit in the fifth position.[22] The peptide, in the following denoted as SSA4WA (Figure 1a), was functionalized at the N terminus with a lipoic group for binding to a gold substrate. Oligopeptides predominantly formed by Aib residues are well known to assume a rigid 3_{10}-helix structure, because of the steric requirements imposed by the *gem*-dimethyl substitution on the C^{α} atom.[23,24]

Although five over six residues of SSA4WA are achiral amino acids (Aib), the only chiral residue (W) is sufficient to bias the secondary structure to a left-handed 3_{10}-helix, as revealed by the characteristic minimum at 208 nm of the circular dichroism (CD) spectrum in ethanol.[22] Ultraviolet (UV)–visible absorption and CD experiments indicate that, under the conditions of the deposition solution (1 mM in ethanol), SSA4WA is predominantly present in solution as a monomeric helical peptide.

The amount of SSA4WA chemisorbed on the gold surface was established by Quartz Crystal Microbalance measurements through the Sauerbrey equation, that is, $\Delta f(\mathrm{Hz}) = -n\Delta m/C$, where n is the order of the vibration of the quartz diskette (typically $n = 1$) and C ($= 1\ \mathrm{ng\,Hz^{-1}}$) is a constant.[25] A frequency variation $\Delta f = 570 \pm 2$ Hz was measured, corresponding to a nominal density of 8.5×10^{-10} peptide moles per cm^2.

Cyclic voltammetry (CV) experiments measuring the discharge of the $[Fe(CN)_6]^{3-}/[Fe(CN)_6]^{4-}$ pair on a bare gold electrode and on gold electrodes coated by SSA4WA or undecanethiol SAMs are reported in Figure 2. Alkanethiol SAMs are known to totally inhibit the discharge of redox active species to modified electrodes. The substantial decrease of the electrochemical activity of the peptide-coated electrode with respect to the bare gold electrode, indicates the formation of a well-packed peptide monolayer and good insulating properties of the peptide film with respect to an external redox species.

A reduction peak associated to the Au–S bond breaking in the peptide SAM was observed at −0.915 V, in agreement with literature data on the reductive desorption of lipoic acid from gold surfaces.[26] Elemental analysis (C, O, N and S) of SSA4WA was carried out by X-ray photoelectron spectroscopy (XPS) measurements on the peptide SAM. The C1s peak contains three components: the

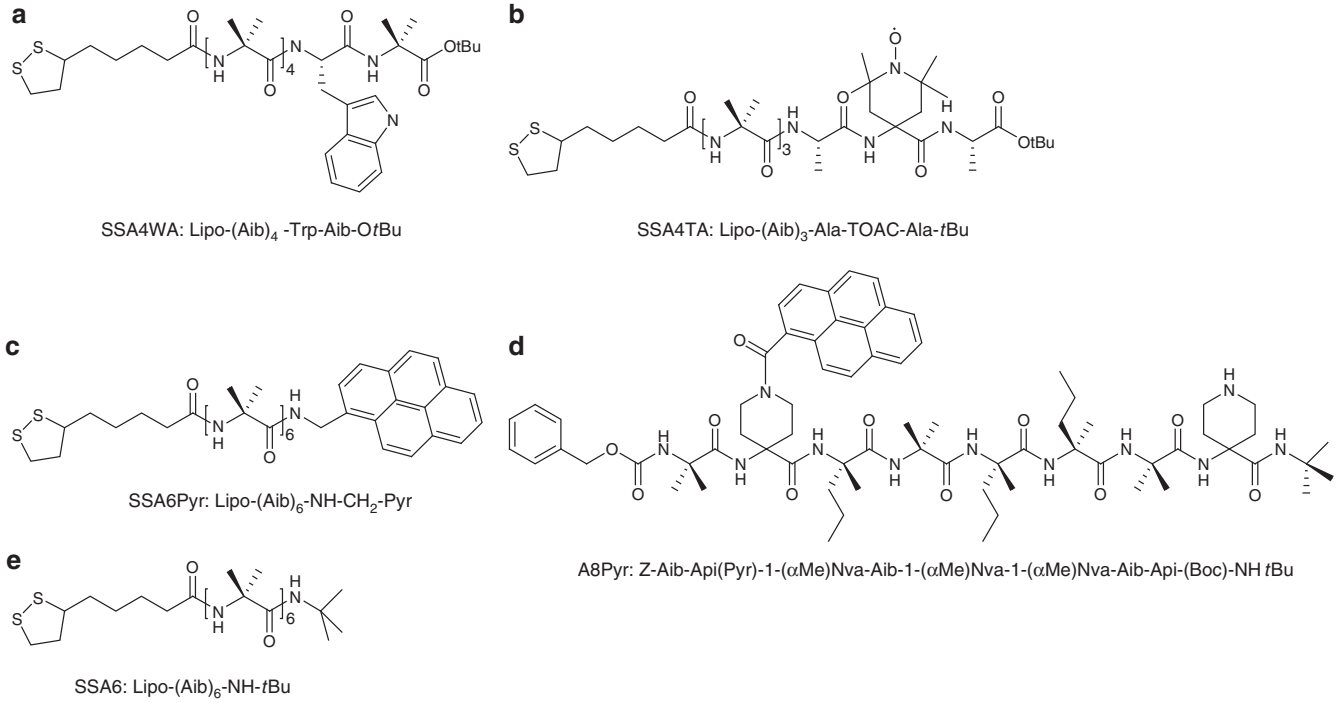

Figure1 Chemical formulas and acronyms of the peptides investigated. (**a**) SSA4WA; (**b**) SSA4TA; (**c**) SSA6Pyr; (**d**) A8Pyr; (**e**) SSA6.

methyl, methylene and methine carbons at 284.9 eV, the C–N/C–O carbons at 286.4 eV, and the carbonyl carbon at 288.0 eV. The normalized areas of the three peaks are 0.80, 0.10 and 0.10, respectively, to be compared with the expected theoretical values of 0.68, 0.16 and 0.16. For O1s, we obtained a single broad peak at 531.1 eV, assigned to carbonyl/carboxyl oxygen atoms. The N1s binding energy was found at 398.2 eV, consistent with an amide group, whereas a second component at 399.8 eV was assigned to the aromatic nitrogen atom of the Trp indole side chain, in agreement with XPS literature data.[27] The normalized areas of the two Gaussian components (0.81 and 0.19) nicely agree with the expected theoretical values (0.86 and 0.14, respectively). Because of the intrinsic low-photoionization cross-section, the signal-to-noise ratio for the S2p peak was rather poor. Nevertheless, its binding energy could be observed at 162.0 eV (0.79), with a minor Gaussian component (0.21) detected at 164.0 eV. Reference data assigned these signals to thiolate atoms chemisorbed on the gold surface and to physisorbed sulfur atoms, respectively.[28]

Scanning tunneling microscopy (STM) imaging of the gold substrate under ultra-high-vacuum (UHV) conditions showed wide atomically flat terraces, separated by steps about 0.2 nm high, corresponding to the Au(111) monoatomic step (0.24 nm). Analysis of the STM images also allowed us to estimate the average roughness of the flat terraces on the gold surface (0.04 ± 0.01 nm). Typical STM images of the gold surface modified by the peptide deposition are shown in Figure 3. In particular, Figures 3a and b display a fairly smooth region of the gold surface homogeneously modified by the chemisorbed peptide. The wide depressions, that is, the dark regions in Figure 3a, originate from pre-existing different structures of the gold surface. The predominant structural feature observed in both the upper layer and within the wide depressions is represented by 'holes', that is, the dark spots magnified in Figure 3b. These holes are 0.2–0.3 nm deep and 2–6 nm wide, as clearly shown by the profile reported in Figure 3c. These features have often been found in SAMs formed by alkanethiols,[29] and have also been observed in STM experiments on peptide SAMs.[30] The occurrence of such structures is considered a good evidence of the formation of a homogeneous peptide monolayer, chemisorbed on the gold substrate through Au–S linkages.[31] Holes originate from the etching of Au atoms from the surface, promoted by the Au–S binding ($E_b = -185\,kJ\,mol^{-1}$), which increases the lateral repulsive pressure of the Au *d*-orbitals.[32]

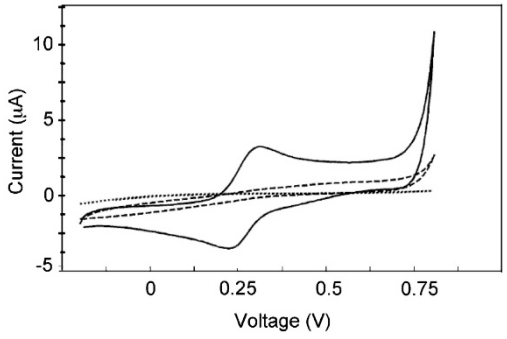

Figure 2 Cyclic voltammetry plots of 1 mM $K_3Fe(CN)_6$ in a 1 M KCl solution. Dashed line: SSA4WA self-assembled monolayer (SAM); dotted line: $C_{11}H_{24}S$ SAM; solid line: unmodified gold electrode (scan speed: $50\,mV\,s^{-1}$). Taken with permission from ref. 22. Copyright © Elsevier.

STM imaging at molecular resolution of alkanethiol films revealed that the small depressions on the gold surface, showing almost circular shape and depth equal to the Au(111) monoatomic step, are densely covered by the alkanethiol SAM.[33]

Current intensity (I) vs applied bias potential (V) spectra of the peptide SAM, obtained by scanning tunneling spectroscopy experiments are reported in Figure 4 together with their associated derivative spectra, that is, dI/dV vs V. All curves were obtained simultaneously to the topographical acquisition, and restricted to a small range of bias voltage ($-1.5/+1.5$ V). The metallic character of the clean gold substrate can be clearly observed by the almost linear I–V curve and the nearly constant value of the I–V derivative (Figure 4a). Curves in Figure 4b were obtained by statistically averaging the I–V signals, taken at selected points of $50 \times 50\,nm^2$ areas of the surface after peptide deposition, and by discriminating between the bright upper layers and the dark large depressions shown in Figure 3a. Both curves exhibited the same behavior, showing a reduction in the metallic character of the modified surface and that the whole surface was homogeneously modified by the peptide. A detailed spectroscopic analysis inside and outside the 'holes' was performed by statistically averaging the I–V signals taken at selected points of $10 \times 10\,nm^2$ areas of the modified surface. The corresponding I–V and dI/dV vs V curves, reported in Figure 4c, did not reveal significant differences, suggesting that peptide molecules were also located into the hole structures.

A different topography of the peptide SAM is shown in Figure 5, where regularly spaced 'stripes' formed by peptide aggregates can be observed. These structures have been found in alkanethiol-based monolayers obtained by vapor deposition,[34] thermal treatment of SAMs prepared by solution deposition[35] and deposition of short-chain alkanethiols.[36] Under these conditions regularly spaced structures with the alkyl chains paralleling the gold surface have been obtained. The STM height profiles reported in Figure 5b show stripe structures 7 nm wide and 0.4 nm high.

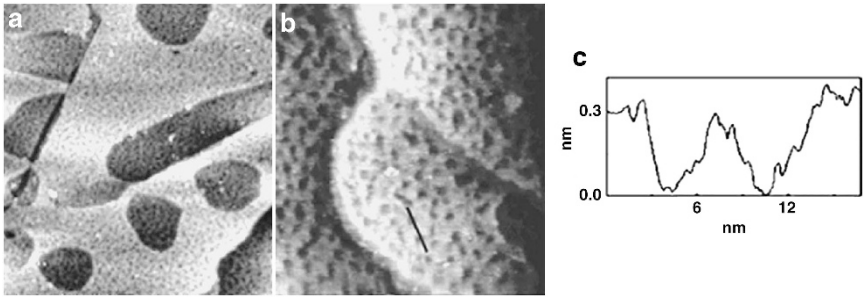

Figure 3 UHV-STM images of the gold surface modified by peptide deposition. (**a**) $200\,nm \times 200\,nm$ ($V = 0.5$ V; $I = 0.5$ nA); (**b**) $100\,nm \times 100\,nm$ ($V = 0.3$ V; $I = 0.8$ nA); (**c**) height profile obtained along the black segment highlighted through two holes in **b**. Taken with permission from ref. 22. Copyright © Elsevier.

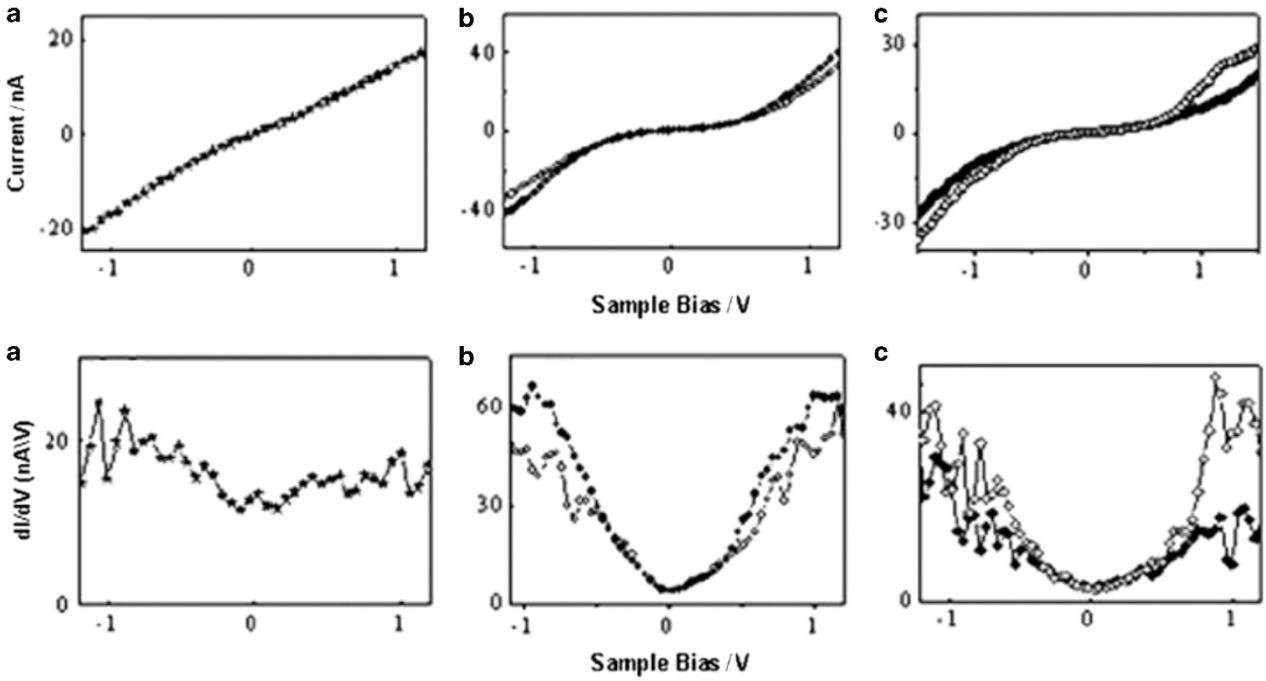

Figure 4 *I*/*V* (upper) and d*I*/d*V* (lower) trend as a function of the applied bias *V*. (**a**) clean gold substrate; (**b**) outside (filled circles) and inside (empty circles) the large depressions imaged on a gold substrate after film deposition; (**c**) outside (filled circles) and inside (empty circles) the holes imaged on a gold substrate after film deposition. Taken with permission from ref. 22. Copyright © Elsevier.

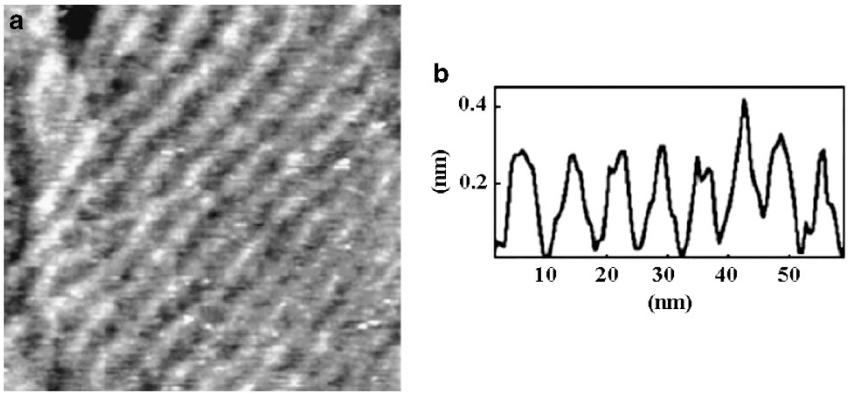

Figure 5 (**a**) 'Stripes' domain revealed by UHV-STM imaging (95 nm × 95 nm); (**b**) height profile taken along the white segment highlighted in the upper part of the figure. The observed 'stripe' structures are about 7 nm wide and 0.2–0.3 nm high ($V = 0.2$ V; $I = 0.8$ nA). Taken with permission from ref. 22. Copyright © Elsevier.

Molecular mechanic calculations reproduced the observed stripe structure considering coupled rows formed by head-to-head peptide dimers, with the sulfur atoms giving rise to a central double row zipping the lying-down peptide layer. The peptide chains were initially located on the gold surface in a 3_{10}-helix conformation or in an extended structure and released to search for the energetically most stable organization. In the former case, we obtained stripe-like structures 4.6 nm wide, whereas in the latter the stripes appear to be separated by 7.0 nm. The latter figure nicely agrees with the STM experimental results, suggesting that favorable van der Waals interactions between the peptide chain and the gold surface induce a structural rearrangement of the peptide chains to form an extended conformation. Because of the steric hindrance exerted by the two C^{β}-methyl groups of the Aib residues, best-packing requirements of these bulky groups and optimization of the van der Waals contacts between the peptide chains and between the peptide chains and the gold surface determine the structural organization of the peptide layer on the surface. Notably, interchain hydrogen bonds cannot form due to steric hindrance of the two C^{β}-methyl groups. Stripe domains may possibly account for the minor fraction of sulfur atoms physisorbed on the gold surface, revealed by XPS measurements. 'Holes' and 'stripes' have already been observed in alkanethiol monolayers at high and low local concentration of alkyl chains, respectively. Depending on the alkyl chain length, temperature and surface coverage, a complex kinetics governs the transition from metastable striped structures to vertically arranged domains coating the gold vacancies.[37] Specifically, stripe domains have been shown to evolve at higher concentrations to a $\sqrt{3}x\sqrt{3}$ R30° structure, with the alkanethiol chains tilted by 30° with respect to the axis perpendicular to the gold surface.[38] Following this structural transition domains of 'holes' are formed. In our case, the reorganization of the peptide stripes into a densely packed, vertically oriented SAM is inhibited by the relatively

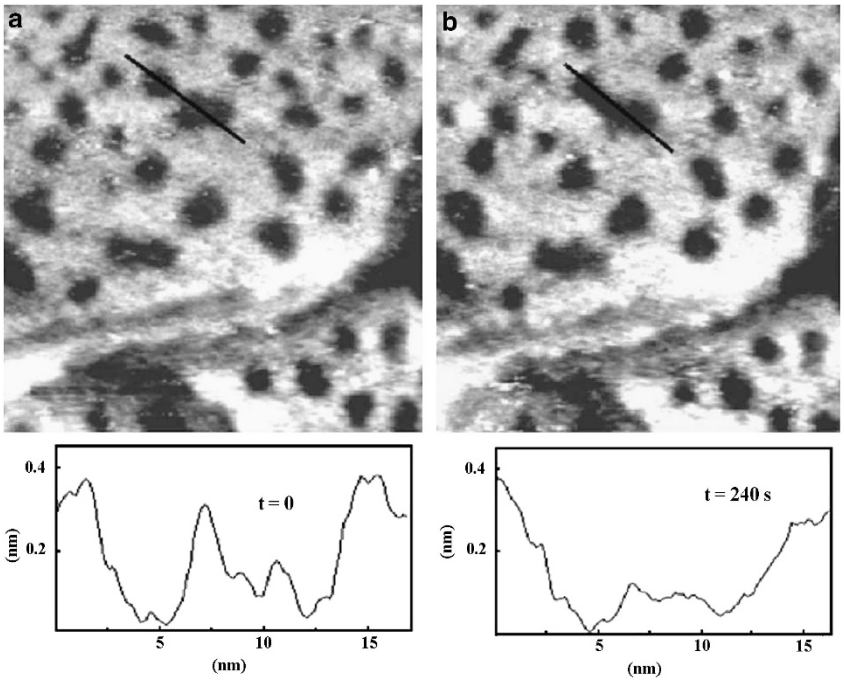

Figure 6 Consecutive STM images (**a** and **b**) of the modified gold surface (delay time $\Delta t = 240$ s). Note the dynamics of the holes marked by the height profiles taken along the segment ruled in the upper figures ($V = 0.2$ V; $I = 0.8$ nA). Taken with permission from ref. 40. Copyright © Elsevier.

weak intermolecular interactions established by the short peptide chains.

DYNAMIC BEHAVIOR OF PEPTIDE-BASED SAMS

The Au–S interaction reveals interesting dynamical features, the Au surface showing large-scale restructuring effects of the surface upon interaction with sulfur ad-atoms. Incorporation of Au atoms into a growing two-dimensional AuS phase was observed *in situ*.[39] The growth mechanism of monolayers of alkanethiols on gold has been shown to consist of nucleation, slow growth and coalescence of vacancy islands in which the chains are densely packed and relatively well ordered.[39] Although surface coverage takes only a few minutes to be achieved, chain ordering dynamics can be very slow, even days, in UHV conditions.[37] The study of the dynamic behavior of SAMs is important in view of the possibility of controlling the growth rates of ordered domains in nanofabrication and microfluidics.

A peculiar behavior of the SSA4WA SAM is the relatively high mobility of the hole structures observed at room temperature and under high-vacuum conditions.[40] The STM images reported in Figures 6a and b refer to two consecutive real-time runs of the tip over the same area. It appears that a diffusional process merging the holes takes place, as clearly shown by the depth profiles reported at the bottom of the figures. The surface mobility of the holes is favored by the weak lateral intermolecular interactions established by the helical peptide chains, the low activation energies associated to the Au–S bond breaking and to the diffusion of Au atoms and/or Au–peptide adsorbates on the surface. Interestingly, in the regions close to the terrace edges and surrounding the large holes, a minor density of holes was observed, a finding implying that the hole coalescence critically depends on their local density on the gold surface.

Small holes generally show an almost circular form, but their coalescence gives rise to elongated structures. A geometrical analysis of the hole perimeter distribution was performed on the STM images of the modified gold surface maintained for 5 days in the sample chamber under UHV conditions. The histogram of the measured perimeters was analyzed in terms of three Gaussian distributions peaked at 7.3 ± 0.8 nm, 12.5 ± 2.0 nm and 19.1 ± 2.9 nm, respectively. This finding is in agreement with earlier results showing that the dimension of the growing elongated structures is roughly proportional to the average size of one, two and three merging holes.[41]

Consensus on the details of the various steps of growth is lacking. The dynamic coalescence model describes the hole growth in terms of: (i) thermal-activated rupture of the Au–S bond, (ii) thermal-activated desorption and diffusion of the gold atoms, followed by (iii) rapid coverage of the atomic vacancies by thiol groups.[37] The signature of Ostwald ripening, a diffusion mechanism involving motion of single Au atoms and Au vacancies, is believed to be the growth of large holes at the expense of small holes.[41] It has also been proposed that mobile thiolate–Au complexes, consisting of the thiolate species linked to a single Au atom, move along the surface as step ad-atoms.[42] Both mechanisms require a concerted motion of Au atoms and thiolate moieties. Healing of SAM defects occurs on a longer time scale (even days) and involves the reorganization of the hydrocarbon chains.[43] This step critically depends on the length of the alkyl chains and it was not observed for chains shorter than 10 carbon atoms. Our STM experiments show that the holes grow by merging with relatively close, small holes and that this diffusional process slows down when a critical local low density is attained or ends when the holes reach a terrace edge (arrested Ostwald ripening).

Summarizing these results, we can conclude that the self-assembly properties of the helical oligopeptide investigated determine the complex morphology of its SAM on the gold surface. The structural organization of the peptide layer on the surface depends on the competition between peptide/surface interactions and the strength of lateral interchain interactions. In spite of the shortness of the peptide chain, SSA4WA gives rise to nanometrically ordered structures, that is, the vertical peptide monolayer coating the 'holes' and the flat dimeric peptide layer arranged horizontally to the gold surface ('stripes'). This

unique behavior can be clearly ascribed to the constrained character of the peptide secondary structure and to the self-assembly properties of the helical chains.

Room temperature diffusion of the holes on the gold surface is favored by the low activation energies required for the rupture of the Au–S bond and migration of gold–peptide adsorbates on the gold surface. Static and dynamic features of SAMs immobilized on a gold surface are intrinsically related. In our case, hole domains, formed by almost vertically arranged peptide helices, predominantly characterize the morphology of the peptide film on the gold surface, whereas stripe domains can be rarely observed. However, after 5 days in UHV conditions, stripe structures can be still detected, the stripe-to-hole transition being probably inhibited by the weak intermolecular interactions established by the short peptide chains.

As helical peptides are well known to act as effective mediators for long range ET,[21,44] the possibility to control the phase structure and growth rates of peptide layers chemisorbed on conductive or semiconductive supports is of paramount importance for the development of molecular devices based on peptide molecular wires.[45] The electronic conductive properties of peptide-based SAMs formed by helical building blocks will be therefore discussed in the next section.

ELECTROCHEMICAL EXPERIMENTS ON PEPTIDE-BASED SAMS

Over the past few years, electrochemical studies and photocurrent generation (PG) experiments on peptides immobilized on metals or semiconductors have become a viable alternative for studying ET processes.[46] The functionalization of the peptide chain at the N terminus with a lipoyl group allows for exploiting the strong Au–S affinity for binding to gold, producing more densely packed peptide SAMs with respect to those formed by C-terminal thiopeptides.[47] As we have shown above, the use of peptides formed almost exclusively by C^{α}-tetrasubstituted amino acids allowed us to obtain rigid helical building blocks even in the case of short oligopeptides. The further functionalization at the C terminus with an electro- or photoactive group, has great advantages in the design of an electrochemical cell based on a working electrode modified by a peptide SAM. This strategy, that is, functionalization at the N terminus with a lipoic group *plus* helical peptide building blocks *plus* functionalization at the C terminus by an electrochemical probe, guarantees that the electroactive group (i) will be sufficiently far from the gold surface to avoid direct gold/probe interaction; (ii) will be accessible to the electrolytic solution; (iii) will be rigidly embedded in the SAM minimizing terminal disordering and chain dynamics effects.

We have recently investigated the electronic conduction properties of an hexapeptide, denoted in the following as SSA4TA, comprising three Aib residues, two Ala residues and a 2,2,6,6-tetramethylpiperidine-1-oxyl-4-amino-4-carboxylic acid (TOAC) residue located at position 5 (Figure 1b).[48] TOAC is a redox-active amino acid,[49] widely used as a probe in electron spin resonance experiments[50,51] or as a quencher of aromatic molecules in fluorescence studies.[52,53] XPS, Fourier-transform infrared absorption and electron spin resonance measurements have shown that this peptide is able to form a stable SAM on a gold substrate, characterized by a thickness of 15 ± 2 Å and with the peptide helical axis tilted by 40° with respect to the normal to the surface.[54] These findings support the view of an almost homogeneous SAM, vertically oriented with respect to the gold surface and quite densely packed.

A typical CV of the SSA4TA SAM is shown in Figure 7, where reversible oxidation/reduction peaks at potential values characteristic of the TOAC group (0.60 V vs SCE) are readily observed. At

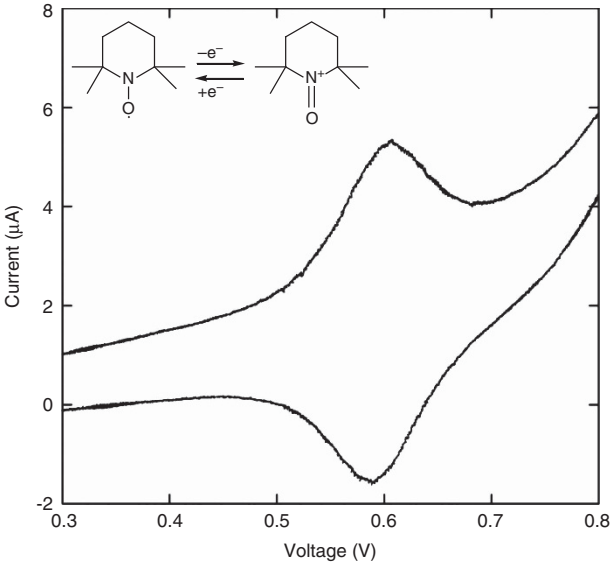

Figure 7 Typical cyclic voltammogram of a gold electrode modified with a SSA4TA self-assembled monolayer at 25 °C (scan rate 0.025 V s^{-1}). Inset: electrochemical reaction of the 2,2,6,6-tetramethylpiperidine-1-oxyl-4-amino-4-carboxylic acid group. Taken with permission from ref. 48 Copyright © Wiley.

sufficiently slow scan rates, typically 0.1 V s^{-1} or slower, reversible conditions are attained and ideal CVs are obtained, in that the observed peak splitting (ΔEp) and peak half-widths are both very small (0 ± 4 and 90 mV, respectively).[55] This result suggests that all redox centers are in a rather homogenous environment, as that provided by an ordered film. CVs of the SSA4TA SAM performed at different sweep rates showed that the oxidative peak current linearly increases with the scan rate, indicating that the observed CV peaks arise from surface-bound TOAC groups.[56]

The electrode surface coverage of the peptide SAM can be obtained from CV experiments by reporting the oxidative or reductive peak intensity, after subtraction of the background (capacitive) current, as a function of the scan rate:

$$I_p(v) = \frac{Nn^2F^2}{4RT}v$$

In the above equation I_p is the anodic (cathodic) peak current, υ the voltage scan rate, N the number of redox-active sites on the surface, n the number of electrons transferred, F the Faraday constant, R the universal gas constant and T the temperature. From the slope of I_p vs υ ($n = 1$), we estimate a surface coverage of 14.4×10^{-11} mol cm^{-2}. This value agrees very well with that theoretically obtained by assuming closely packed and vertically arranged 3_{10}-helical peptide chains, that is, 16.6×10^{-11} mol cm^{-2}.[57]

Chronoamperometry experiments were also carried out for characterizing the rate of ET from TOAC to the gold electrode across the peptide SAM. In ET reactions between surface-bound redox groups and metal electrodes, the current I is expected to decay exponentially with time, according to the equation:

$$I(t) = I_0 e^{-k_{ET}t}$$

where I_0 is the current at $t = 0$ and k_{ET} is the ET rate constant.

Experimental I—t curves for SSA4TA in the 2–200 μs time region were therefore analyzed to determine k_{ET} at different positive overpotentials, that is, the difference between the applied potential and the standard redox potential of TOAC. The ET rate constants measured

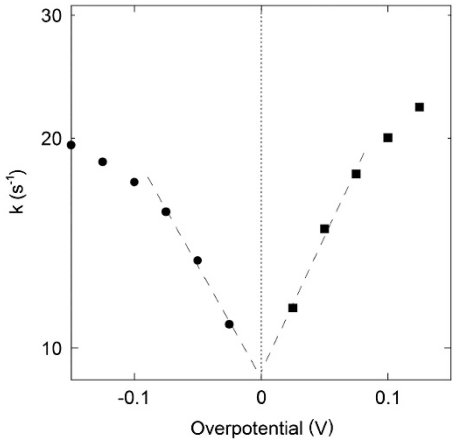

Figure 8 Dependence of the electron transfer (ET) rate constant (k_{ET}) on the applied overpotential (*V*) for 2,2,6,6-tetramethylpiperidine-1-oxyl-4-amino-4-carboxylic acid (TOAC) oxidation (filled squares) and $TOAC^+$ reduction (filled circles) at the gold electrode through the SSA4TA self-assembled monolayer. Taken with permission from ref. 48. Copyright © Wiley.

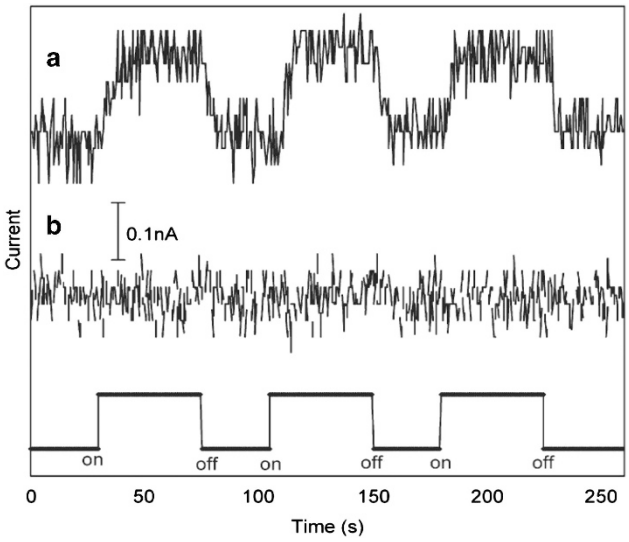

Figure 9 Time course of photocurrent intensity for (**a**) peptide self-assembled monolayer (SAM)-modified IDE; (**b**) interdigitated gold microelectrode modified by the undecanethiol SAM. Applied potential vs Ag/AgCl: 0 V; $\lambda_{exc} = 280$ nm. Taken with permission from ref. 66. Copyright © Elsevier.

for the TOAC oxidation at positive overpotentials and those for the $TOAC^+$ reduction at negative overpotentials (Tafel plot) are shown in Figure 8. A strong dependence of the ET rate constants on the applied potential was observed, similar to that found in the case of SAMs composed of alkanethiols or other sulfur-terminated compounds.[58] The ET rate constant at the standard redox potential was determined by extrapolating the data of Figure 8 to a null overpotential, obtaining $k_{ET} = 9.2\,s^{-1}$ for ET from TOAC to gold and $k_{ET} = 9.3\,s^{-1}$ for back ET from gold to $TOAC^+$. This finding confirms the reversibility of the ET process.

The *along-the-molecule* distance between the TOAC group and the gold surface can be roughly estimated to be 17 Å, obtained by summing the molecular length of the peptide backbone in a rigid 3_{10}-helix arrangement (≈ 2.0 Å rise per residue) to the lipoyl chain in an all-*trans* conformation (7.3 Å). At this distance, the tunneling (SE) mechanism, which is characterized by an exponential dependence of the ET rate constant on the distance and by a strong dependence on the overpotential, most likely predominates.

Interestingly, the Tafel plot (Figure 8) shows a marked asymmetry of the k_{ET} vs applied bias potential curves obtained in oxidative and reductive conditions. This effect was ascribed to the electrostatic field generated by the electric macrodipole associated with the helical peptide chain. At positive overpotentials, electrons are transferred from TOAC to the gold electrode (k_a), that is, from the C terminus to the N terminus, whereas for negative overpotentials, ET occurs in the opposite direction (k_c), that is, from the N terminus to the C terminus. As the electric macrodipole is directed from the C terminus ($\delta -$) to the N terminus ($\delta +$), k_a at a given overpotential is expected to be higher than k_c. From the data reported in Figure 8, k_a/k_c is 1.19 ± 0.05. This value is definitely smaller than that observed in α-helical peptides,[59] suggesting that the electric field effect on the ET process in 3_{10}-helical peptides is less important, probably because of the distortion of the hydrogen-bond network with respect to the helical axis. This result is consistent with that obtained by time-resolved fluorescence measurements for photoinduced ET in 3_{10}-helical peptides in solution.[60]

PG EXPERIMENTS ON PEPTIDE-BASED SAMS

Despite intense research efforts, the importance of competitive mechanisms governing ET across peptide matrices is still strongly debated.[21,46] In the SE model, the peptide chain mediates the coupling between the donor and the acceptor pair through electronic virtual states, whereas in the alternative hopping mechanism the electron jumps through the single-amino-acid residues with a finite time of residence on each bridging unit. The amide bond has been proposed as the site of residence of the transferred electron, and the role of aromatic side chains as electron sink was recently unequivocally demonstrated.[61] Both mechanisms are thought to be operative (and to compete as well) at all distances. However, for short peptides ($n \leqslant 10$) and donor–acceptor distances shorter than 20 Å, SE mechanism was shown to predominate.[62,63]

However, the overwhelming majority of such studies were carried out in solution on peptides functionalized with an ET donor–acceptor pair. The understanding of ET or photoinduced ET across peptide chains in organic/inorganic hybrid systems is at the moment less clearly established, due to the complexity of the occurring physical processes and the paucity of experimental data.

Recently, PG experiments have become the method of choice for studying ET processes across a peptide SAM, due to the unique electronic conduction properties of peptides in terms of long-range and directional ET. PG experiments through peptide SAMs have been actively investigated by Kimura and co-workers[14,47,64,65] who focused on the dependence of the ET efficiency on the peptide length, type of secondary structure, pH, role of aromatic residues, electronic coupling through the amino-acid bridging units.

As we have shown in the previous sections, the introduction of conformationally constrained residues in the peptide chain affords the great advantage to control the peptide secondary structure, thus modulating the separation between the photoactive group and the gold surface.

We therefore carried out PG experiments using an interdigitated gold microelectrode (IDE) modified by the deposition of the SSA4WA SAM. An anodic current was obtained by photoexcitation in the Trp absorption region and using TEOA as an electron donor in the electrolytic solution.[66] In Figure 9, typical photocurrent signals obtained upon photoirradiation at 280 nm of the peptide-modified

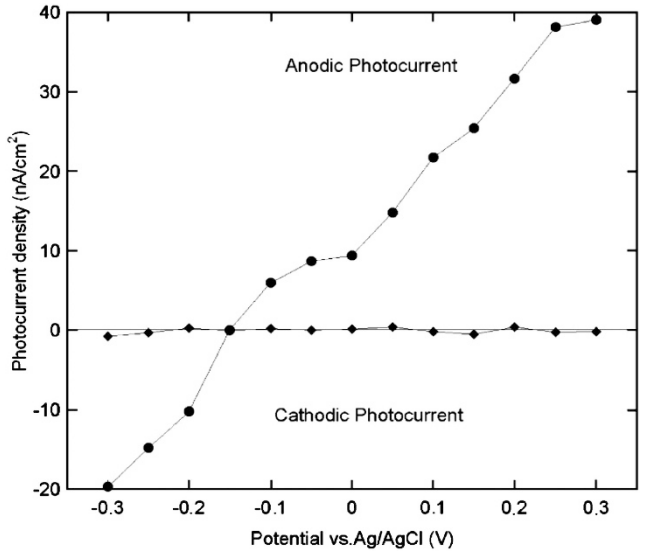

Figure 10 Photocurrent density for different applied potentials (V) at $\lambda_{exc} = 280$ nm. Full circles: peptide self-assembled monolayer (SAM)-modified interdigitated gold microelectrode (IDE); diamonds: undecanethiol SAM-modified IDE. Taken with permission from ref. 66. Copyright © Elsevier.

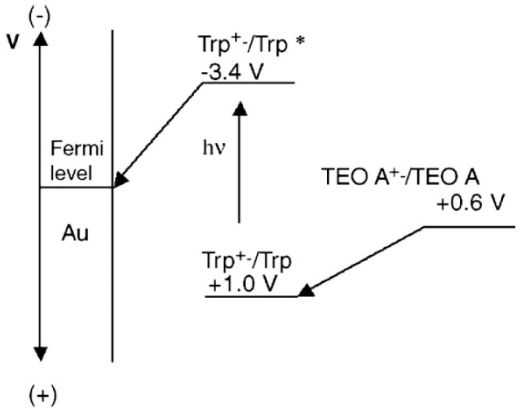

Figure 11 Energy diagram for anodic photocurrent generated by the peptide self-assembled monolayer in the presence of the TEOA electron donor. Taken with permission from ref. 66. Copyright © Elsevier.

IDE were reported. Photocurrent measurements on an IDE modified by an undecanethiol SAM in the same experimental conditions were also reported for reference.

The anodic photocurrent measured for the peptide-modified IDE can be clearly seen, as opposed to the null response of the undecanethiol gold electrode. Interestingly, the measured photocurrent intensity follows reversibly the on/off photoexcitation cycles without apparent degradation of the anodic current. When the peptide layer is irradiated in the UV range between 260 and 320 nm, the indole group gives rise to ET from its singlet excited state to the surface Fermi level of the Au electrode. Subsequently, TEOA transfers an electron to Trp, giving rise to a net, anodic, electronic current. Photocurrent intensity vs applied potential voltage (P/V) experiments were also carried out at the Trp maximum absorption wavelength ($\lambda_{max} = 280$ nm; Figure 10).

The photocurrent efficiency is quantitatively taken into account by introducing the incident photon-to-current efficiency (IPCE%) factor, that is, the ratio of the electrons injected in the external circuit to the number of incident photons. This quantity can be evaluated from the equation:[67]

$$\text{IPCE } \% = 100\frac{1240 i_{sc}}{\lambda_{exc} i_{inc}}$$

where i_{sc} is the short circuit photocurrent ($A\,cm^{-2}$), I_{inc} the incident light intensity ($W\,cm^{-2}$) and λ_{exc} the excitation wavelength (nm). At 0 V applied potential, the measured IPCE% is 0.015 at 280 nm. The peculiar P/V dependence of the peptide-modified IDE is most evident, as opposed to the null P/V curve of the undecanethiol IDE (Figure 10).

For the peptide-modified IDE, a decrease in the anodic photocurrent with an increase of the negative bias to the working electrode was observed, measuring a null photocurrent at a given, characteristic potential (zero-current potential, zcp). The negative bias reduces the energy gap between the oxidation potential of Trp excited state (Trp*) and the gold Fermi level, resulting in the decrease of the anodic photocurrent. Notably, the anodic photocurrent changes to a cathodic one by applying a negative bias larger than zcp. It was suggested that, in this case, an electron acceptor species (H^+) in solution may accept an electron from a photoexcited Trp group to generate a cathodic photocurrent.[47] At zcp, the opposing photocurrents cancel each other out, leading to an apparent null current state. Interestingly, the SSA4WA SAM shows a negative zcp value (-0.15 V), most likely determined by the negative potential around the indole group generated by the helix dipole.

These considerations are summarized by the energy diagram sketched in Figure 11, where the anodic PG process is split in two ET steps: (i) a Trp* → Au ET step mediated by the bridging peptide chain and (ii) a TEOA → $Trp^{+\cdot}$ (radical cation) diffusion-controlled ET reaction. The former most likely represents the rate-limiting step because of the long distance between the donor (Trp) and the acceptor (metal surface). Thus, the quantum efficiency of PG is mainly determined by ET across the peptide chain.

It should be stressed that the peptide SAM packing and homogeneity are not perturbed by photoirradiation, as proved by CV measurements on the same sample before and after several cycles of photocurrent experiments.

By irradiation in the far-UV region ($\lambda_{exc} < 250$ nm), an intense anodic photocurrent was measured also in the case of a bare gold electrode in contact with a TEOA solution, as a result of direct photoelectric ejection from gold (the Au work function is 5.1 eV, corresponding to 243 nm) and ET from photoexcited triethanolamine to gold (TEOA* → Au). These drawbacks can be only partially removed, due to the overlap of the $n \rightarrow \pi^*$ transition of Trp to the tail of the gold and TEOA absorption.

For this reason, we decide to investigate the PG properties of an hexapeptide, denoted in the following as SSA6Pyr (Figure 1c), having the same amino-acid composition, that is, six consecutive Aib residues and a lipoyl group at the N terminus for covalent binding to gold, but functionalized at the C terminus by a pyrene group, a chromophore absorbing in the near UV and strongly emitting in the blue region of the visible spectrum. CV experiments confirmed that also SSA6Pyr, despite the shortness of the peptide chain, can form a densely packed SAM on the gold electrode, inhibiting almost completely the discharge of $K_3[Fe(CN)_6]$.[68]

The photocurrent generated upon photoirradiation of the SSA6Pyr SAM in the presence of TEOA is shown in Figure 12, where repeated on/off cycles of photoexcitation, each one 30 s long, are reported for different excitation wavelengths.[69]

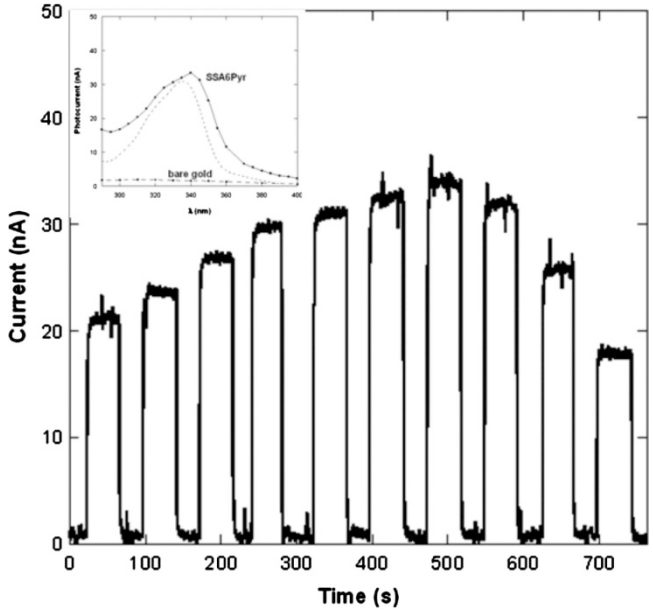

Figure 12 Time course of the photocurrent of the SSA6Pyr self-assembled monolayer (SAM) in an aqueous TEOA solution at 0 V vs Ag/AgCl upon photoirradiation at different wavelengths (from 310 to 355 nm every 5 nm, 15 nm bandwidth) at room temperature. Inset: action spectrum of the SSA6Pyr SAM (solid line with dots) as compared with the action spectrum of the bare gold electrode (dashed line with dots) and the fluorescence excitation spectrum of pyrene in acetonitrile (solid line). Taken with permission from ref. 69. Copyright © Wiley.

The action spectrum, that is, the photocurrent response vs the excitation wavelength, of the SSA6Pyr SAM shows a very good agreement with the absorption spectrum of pyrene in ethanol solution (inset of Figure 12). The null signal shown by the bare gold electrode emphasizes the role of the pyrene chromophore as ET photosensitizer (*antenna effect*).

When PG experiments were conducted on a gold electrode modified by deposition of an SSA6Pyr SAM in an aqueous solution of methyl viologen (MV^{2+}), a well-known electron acceptor molecule,[14,47] a cathodic photocurrent was obtained upon irradiation in the same UV range at 0 V applied potential. The photocurrent action spectrum of the peptide SAM indicates that, in these experimental conditions, the pyrenyl group photosensitizes ET from gold to MV^{2+}.

At 0 V applied potential, the IPCE% of the SSA6Pyr SAM was 0.04% at the pyrene absorption maximum ($\lambda_{exc} = 340$ nm). A comparison between the anodic and cathodic photocurrent responses shows a sevenfold increase in the IPCE% for the anodic current compared with the cathodic one. This effect is most likely determined by the electric field generated by the helix dipole, as already found by us for ET in solution through 3_{10}-helical peptides[60] and in chronoamperometry experiments on electrodes modified by peptide SAMs,[48] as discussed above. This is because, in PG experiments in anodic conditions (TEOA in solution), the electrons flow across the peptide chain from the C terminus to the N terminus (oxidation process), whereas in cathodic conditions (MV^{2+} in solution), ET takes place in the opposite direction, that is, from the N terminus to the C terminus (reduction).

These findings pave the way to the possibility of realizing a molecular photodiode able to switch the current direction by changing the electrolyte in solution and tuning the applied bias potential, as already shown by Kimura and co-workers[14] in a proof of principle experiment. These results confirm the unique electron-mediating properties of helical peptides, making them very promising materials for use in bioelectronics.

SOFT ENGINEERING OF BICOMPONENT PEPTIDE SAMS

Recently, Kimura and co-workers[14] demonstrated that the immobilization of a bicomponent SAM composed of two helical peptides in which the gold binding (S,R) lipoic group was linked either at the C- or at the N-terminus, respectively, can generate a more densely packed monolayer as compared with a SAM, in which the helical peptide macrodipoles are aligned in a parallel way. This effect was ascribed to the attractive interchain interactions taking place between opposing helical macrodipoles in the bicomponent SAM. Kraatz and co-workers[70,71] also demonstrated that, even if peptide SAMs are dynamical systems, in the antiparallel dipole arrangement, the peptide chains experience a more restricted motion due to stronger intermolecular interactions. The assembly of supramolecular structures on the basis of the intermolecular interaction of molecular electric dipoles (*molecular dipole engineering*) has been therefore proposed as a promising tool for the design of nanomaterials and nanodevices.[72]

Very recently, we proposed a soft-engineering approach showing that it is possible to immobilize a photoactive peptide lacking sulfur atoms on a gold surface by exploiting weak intermolecular interactions.[73] To this aim, we studied a conformationally constrained 3_{10}-helical octapeptide based on the C^{α}-tetrasubstituted Aib, Api (4-aminopiperidine-4-carboxylic acid) and L-(αMe)Nva (C^{α}-methyl norvaline) residues. The new peptide was functionalized in the proximity of the N terminus by a 1-pyrenyl (Pyr) unit, but was deprived of lipoic or other S-containing groups (A8Pyr, Figure 1d). It should be noted that L-(αMe)Nva is a chiral amino acid, and this allowed us to confirm the helical structure of A8Pyr by CD measurements.

A bicomponent SAM, composed of SSA4WA, covalently linked to the gold surface through Au–S interaction, and A8Pyr, tethered into the SSA4WA palisade, has been therefore obtained by overnight deposition of a 0.5 mM $3{:}1_{(v/v)}$ ethanol/water equimolar solutions of the two peptides on a gold electrode. It was expected that the antiparallel arrangement of the two peptide foldamers (SSA4WA has necessarily its positive end dipole directed toward the gold surface) favors the inclusion of A8Pyr into the SSA4WA SAM with the positive end of the helix dipole pointing toward the SAM outer surface. Importantly, in this arrangement both the Pyr and Trp chromophores would be located at the outer surface of the SAM and in contact with the electrolytic solution. CV experiments carried out on a gold electrode modified by an A8Pyr/SSA4WA SAM in an aqueous $K_3Fe(CN)_6$ solution showed that the electrolyte discharge at the electrode is almost completely inhibited, indicating the dense packing of the bicomponent SAM on the gold surface.

To characterize the optical properties of the bicomponent SAM, fluorescence spectra were measured on a glass support coated with a 5-nm thick gold layer.[69] In particular, the emission of the pyrene fluorescent probe in the SAMs formed by A8Pyr with SSA4WA and SSA6, an homoAib hexapeptide lacking the pyrene probe (Figure 1e) was carefully investigated. Pyrene is a spatially sensitive fluorophore, which forms excited-state dimers (excimers) upon a close encounter with another Pyr-based molecule.[74] Therefore, the observation of excimer emission signals the onset of close range Pyr–Pyr interactions in the peptide SAMs, and, in case of a bicomponent SAM may

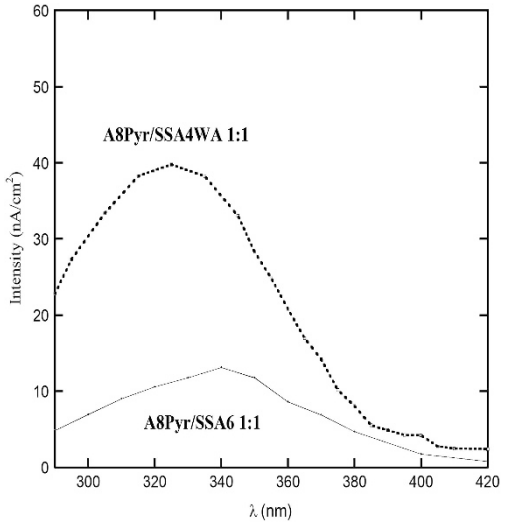

Figure 13 Photocurrent action spectra in the Pyr absorption region of gold electrodes modified by: 1:1 A8Pyr/SSA4WA (dashed line) and 1:1 A8Pyr/SSA6 (full line) self-assembled monolayers. Applied potential: 0 V vs Ag/AgCl in all cases. The spectra were normalized to the electrode geometric surface and the exciting source intensity. Taken with permission from ref. 69. Copyright © Wiley.

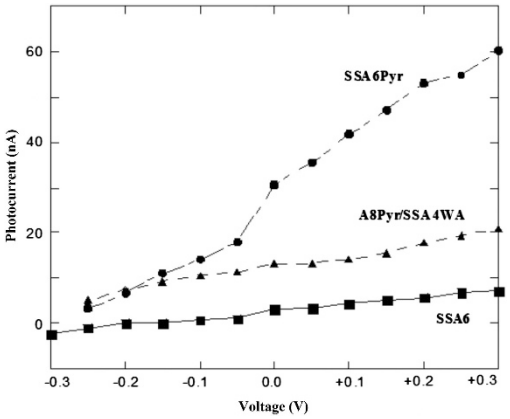

Figure 14 Photocurrent generated by SSA6Pyr (full circles), A8Pyr/SSA4WA (full triangles) and SSA6 (full squares) peptide self-assembled monolayers by excitation at 340 nm as a function of the applied bias potential. The slope of the reported curves is proportional to the electronic coupling between the electron donor and the electrode density of states, mediated by the peptide chain. Taken with permission from ref. 69. Copyright © Wiley.

indicate, the formation of raft domains, that is, segregated single-component regions.

The emission spectrum of the 1:1 A8Pyr/SSA4WA is characteristic of the Pyr monomer emission, suggesting that A8Pyr and SSA4WA are homogeneously intercalated in the bicomponent SAM.[69,73] On the other hand, the emission spectrum of the A8Pyr/SSA6 SAM revealed a significant contribution of excimer-like species. In this case, the relatively free dynamics of A8Pyr in the less organized SAM formed by SSA6, most likely allowed for the formation of local domains rich in A8Pyr. The reported fluorescence experiments, besides confirming the inclusion of A8Pyr in both the SSA4WA and SSA6 SAMs, nicely parallel the CV results and confirm the formation of a densely packed A8Pyr/SSA4WA SAM.

The photocurrent action spectra of the SAMs formed by A8Pyr with SSA4WA and SSA6 in the Pyr absorption region are reported in Figure 13. The antenna effect of the Pyr chromophore is emphasized by the almost null photocurrent measured for the SSA6 SAM. In the latter case, the measured weak photocurrent can be ascribed to a photothermal effect, that is, a potential drop caused by heating of the diffusion layer at the electrode interface upon illumination, recently discussed by Kraatz and co-workers.[75]

The observation of a photocurrent action spectrum identical to that measured for the SSA6Pyr SAM confirmed the photoactivity of the Pyr chromophore in both the 1:1 A8Pyr/SSA4WA and 1:1 A8Pyr/SSA6 SAMs (Figure 13). However, the photocurrent intensities measured for the latter SAMs are definitely less intense than those measured in the case of peptides functionalized with the same Pyr chromophore, but covalently linked to the gold surface through the lipoic group.

To investigate the role of the Au–S linkage at the peptide–gold interface in determining the efficiency of the ET process, the dependence of the anodic photocurrent on the applied potential was analyzed at the Pyr maximum excitation wavelength ($\lambda = 340$ nm) for the SSA6Pyr and the A8Pyr/SSA4WA peptide SAMs (Figure 14). The same analysis was also carried out for the SSA6 SAM as a control experiment. In all cases, a decrease of the anodic photocurrent intensity was observed upon reducing the positive bias voltage to the working electrode, measuring a null photocurrent at a characteristic potential (zcp). This result is due to the fact that the less positive the applied bias, the smaller is the energy gap between the Pyr* oxidation potential and the gold electrode Fermi level, that is, the ET driving force in the normal Marcus region.

The slope of the *P*/*V* curve depends on the electronic coupling between the molecular HOMO/LUMO energies of the antenna chromophore and the density of the metal electronic states across the peptide bridge, that is, the tunneling matrix H_{AD}.[76] The observed linear dependence of the generated photocurrent on the applied potential emphasizes the role of the peptide matrix in the ET process, but it does not allow *per se* to distinguish between a coherent tunneling (SE) and a diffusive hopping mechanism, because both ET models were shown to be linearly dependent on the applied potential at low voltages.[76] Figure 14 shows that the slope of the *P*/*V* curve for the SSA6Pyr SAM is definitely steeper than that measured for the A8Pyr/SSA4WA SAM. This finding may be ascribed to the different types of interaction established by the two SAMs at the peptide–gold interface (*junction effect*). The Au–S junction, an almost chemical bond ($\approx 40\,\text{kcal}\cdot\text{mol}^{-1}$) to which the peptide helix dipole confers a partial polar character with the positive end at the gold surface ($Au^{\delta+}$–$S^{\delta-}$), allows for a through-bond ET pathway across the peptide chain, characterized by a relatively low activation energy at the gold–peptide interface.

This pathway cannot operate for A8Pyr, which lacks the disulfide group and is firmly embedded into the bicomponent SAM by favorable interchain interactions with SSA4WA. In the latter case, direct $Pyr^* \rightarrow Au$ ET across the A8Pyr peptide chain would necessarily require a through-space jump from the peptide N terminus to the gold surface, a step characterized by a relatively high activation energy. Furthermore, the A8Pyr helix dipole moment is directed in the bicomponent SAM with the negative end pointing toward the gold electrode, and this would definitely hinder ET in that direction. A possible alternative pathway may proceed through an initial intermolecular ET step from the excited Pyr to the Trp group ($Pyr^* + W \rightarrow Pyr^{+\bullet} + W^-$) or to the amide site of a nearby peptide chain, followed by ET across the Au–S-linked peptide chain from the Trp or the peptide radical to the gold surface. This second step should be also favored by the electrostatic field generated by the peptide helix.

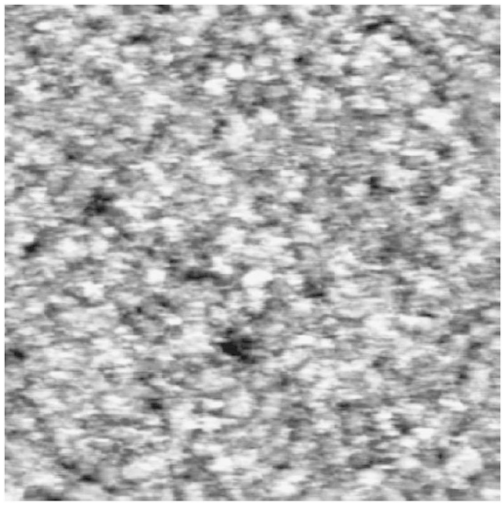

Figure 15 Constant current STM image of the A8Pyr/SSA4WA self-assembled monolayer. Many bright spots were observed. The diameter of each spot is 1 nm. This image was recorded with a sample bias of 3.8 V and a tunneling current set of 60 pA. Taken with permission from ref. 73. Copyright © American Chemical Society.

This view was supported by UHV-STM measurements on the A8Pyr/SSA4WA SAM performed at a bias voltage of 3.8 V (Figure 15). Many bright spots, showing a diameter of 1 nm and protruding by approximately 2.0 ± 0.5 Å from the surrounding matrix, were clearly observed at highly positive bias voltages.

The diameter of the dots found in the STM measurements well agrees with that of a 3_{10}- helix (ca 1 nm), letting us to consider each dot as representing a single-helical peptide protruding from the surrounding peptide SAM. Because of the presence of the Pyr moiety, A8Pyr is characterized by a higher electron density at the SAM outer surface with respect to SSA4WA. For this reason, we assigned the observed bright spots to the Pyr-containing molecules.[73] This finding strongly suggests that SSA4WA and A8Pyr form a densely packed and homogeneously distributed SAM, where the former hexapeptide is bound to gold through the N-terminal lipoic group, and the latter octapeptide is embedded into the SSA4WA palisade in an antiparallel arrangement, protruding from the SSA4WA layer.

Interestingly, the IPCE measured for the A8Pyr/SSA4WA SAM (IPCE = 0.02%) is definitely greater than that measured for the A8Pyr/SSA6 SAM (IPCE = 0.006%), suggesting an important contribution of the Trp group to the interchain ET process. In any case, the photocurrents generated by the A8Pyr/SSA4WA and A8Pyr/SSA6 SAMs are both definitely greater than that measured for the SSA6 SAM (IPCE = 0.002%), emphasizing the role of the Pyr antenna even in the case of a peptide not covalently linked to the gold surface.

CONCLUSIONS

The main achievement of our studies is the proof that is possible to form densely packed and stable SAMs by using helical oligopeptide building blocks. This result was made possible by the particular nature of the peptides investigated, able to attain helically ordered conformations despite the shortness of their main chain. This property, in turn, is due to the unique conformational properties of their amino-acid components, that is, the C^{α}-tetrasubstituted residues.

The second important result is that peptides suitably functionalized with electro- or photoactive groups can form ordered nanometric films, with possible application in the fields of sensing, molecular recognition and bioelectronics.

In our studies peptide SAMs have represented simple and well-defined models for studying ET processes in hybrid devices, and specifically ET at a metal-organic layer interface. In particular, we have shown that it is possible: (i) to modulate the efficiency of the ET process by functionalizing the peptide scaffold with a suitable chromophore (*antenna effect*), (ii) to form bicomponent peptide SAMs by exploiting favorable interchain interactions between the helix macrodipole, (iii) to open additional ET pathways promoted by lateral interchain interactions in bicomponent SAMs and (iv) to tune the coupling between the photoactive layer and a conductive substrate by changing the nature of the interface (covalently linked or physically adsorbed) embedding the electron donor states (*junction effect*). These findings could be of remarkable relevance for the design of new bioinspired materials for nanoelectronics and optoelectronic devices based on conductive organic thin films.

ACKNOWLEDGEMENTS

We thank the Laboratory of Peptide Synthesis of the Department of Chemistry of the University of Padova, headed by Professor Claudio Toniolo, for the synthesis of all the peptides reported in this review. We also thank Professor Antonio Palleschi, Professor Lorenzo Stella, Dr Gianfranco Bocchinfuso and Professor Basilio Pispisa (University of Rome Tor Vergata) who contributed to this work in many aspects. We also acknowledge the funding of this research by the Italian Ministry for Instruction, University and Research (MIUR, PRIN 2010-2011 n. 2010FM738P—Photophysical and photochemical properties of organic and biological compounds in solution and in organized systems).

1 Lehn, J.-M. Toward complex matter: supramolecular chemistry and self-organization. *Proc. Natl Acad. Sci. USA* **99,** 4673–4678 (2002).
2 Love, J. C., Estroff, L. A., Kriebel, J. K., Nuzzo, R. G. & Whitesides, G. M. Self-assembled monolayers of thiolates on metals as a form of nanotechnology. *Chem. Rev.* **105,** 1103–1170 (2005).
3 Stupp, S. F. Introduction: functional nanostructures. *Chem. Rev.* **105,** 1023–1024 (2005).
4 Langer, R. & Tirrell, D. A. Designing materials for biology and medicine. *Nature* **428,** 487–492 (2004).
5 Zhang, S. Fabrication of novel materials through molecular self-assembly. *Nat. Biotechnol.* **21,** 1171–1178 (2003).
6 Fendler, J. H. Chemical self-assembly for electronic applications. *Chem. Mater.* **13,** 3196–3210 (2001).
7 Ulman, A. Formation and structure of self-assembled monolayers. *Chem. Rev.* **96,** 1533–1554 (1996).
8 Chaki, N. K. & Vijayamohanan, K. Self-assembled monolayers as a tunable platform for biosensor applications. *Biosens. Bioelectr.* **17,** 1–12 (2002).
9 Gellman, S.H. Foldamers: A manifesto. *Acc. Chem. Res.* **31,** 173–180 (1998).
10 Toniolo, C., Crisma, M., Formaggio, F. & Peggion, C. Control of peptide conformation by the Thorpe-Ingold effect (C^{α}-tetrasubstitution). *Biopolym. Pept. Sci.* **60,** 396–419 (2001).
11 Loo, Y., Zhang, S. & Hauser, C. A. E. From short peptides to nanofibers to macromolecular assemblies in biomedicine. *Biotechn. Adv.* **30,** 593–603 (2012).
12 Badia, A., Lennox, R. B. & Reven, L. A dynamic view of self-assembled monolayers. *Acc. Chem. Res.* **33,** 475–481 (2000).
13 Galoppini, E. & Fox, M. A. Effect of the electric field generated by the helix dipole on photoinduced intramolecular electron transfer in dichromophoric α-helical peptides. *J. Am. Chem. Soc.* **118,** 2299–2300 (1996).
14 Yasutomi, S., Morita, T., Imanishi, Y. & Kimura, S. A molecular photodiode system that can switch photocurrent direction. *Science* **304,** 1944–1947 (2004).
15 Fujita, K., Bunjes, N., Nakajima, K., Hara, M., Sasabe, H. & Knoll, W. Macrodipole interaction of helical peptides in a self-assembled monolayer on gold substrate. *Langmuir* **14,** 6167–6172 (1998).
16 Sek, S., Sepiol, A., Tolak, A., Misicka, A. & Bilewicz, R. Distance dependence of the electron transfer rate through oligoglycine spacers introduced into self-assembled monolayers. *J. Phys. Chem. B* **108,** 8102–8105 (2004).
17 Uvdal, K. & Vikinge, T. P. Chemisorption of the dipeptide Arg-Cys on a gold surface and the selectivity of G-protein adsorption. *Langmuir* **17,** 2008–2012 (2001).
18 Worley, C. G., Linton, R. W. & Samulski, E. T. Electric-field-enhanced self-assembly of α-helical polypeptides. *Langmuir* **11,** 3805–3810 (1995).

19 Niwa, M., Morikawa, M. & Higashi, N. Discrimination between N- and C-termini of polypeptides by a two-dimensional array of helical poly(L-glutamic acid) rods on gold surfaces. *Langmuir* **15,** 5088–5092 (1999).
20 Miura, Y., Kimura, S., Kobayashi, S., Iwamoto, M., Imanishi, Y. & Umemura, U. Negative surface potential produced by self-assembled monolayers of helix peptides oriented vertically to a surface. *Chem. Phys. Lett.* **315,** 1–6 (1999).
21 Morita, T. & Kimura, S. Long-range electron transfer over 4 nm governed by an inelastic hopping mechanism in self-assembled monolayers of helical peptides. *J. Am. Chem. Soc.* **125,** 8732–8733 (2003).
22 Venanzi, M., Pace, G., Palleschi, A., Stella, L., Castrucci, P., Scarselli, M., De Crescenzi, M., Formaggio, F., Toniolo, C. & Marletta, G. Densely-packed self-assembled monolayers on gold surfaces from a conformationally constrained helical hexapeptide. *Surf. Sci.* **600,** 409–416 (2006).
23 Toniolo, C. & Benedetti, E. The polypeptide 3_{10}-helix. *Trends Biochem. Sci.* **16,** 350–353 (1991).
24 Toniolo, C., Polese, A., Formaggio, F., Crisma, M. & Kamphuis, J. Circular dichroism spectrum of a peptide 3_{10}-helix. *J. Am. Chem. Soc.* **118,** 2744–2745 (1996).
25 Sauerbrey, F. Verwendung von schwingquarzen zur wägung dünner schichten und zur mikrowägung. *Z. Phys.* **155,** 206–222 (1959).
26 Cheng, Q. & Brajter-Toth, A. Permselectivity, sensitivity, and amperometric pH sensing at thioctic acid monolayer microelectrodes. *Anal. Chem.* **68,** 4180–4185 (1996).
27 Cao, X., Coulter, S. K., Elison, M. D., Liu, H., Liu, J. & Hamers, R. J. Bonding of nitrogen-containing organic molecules to the silicon (001) surface: the role of aromaticity. *J. Phys. Chem. B* **105,** 3759–3768 (2001).
28 NIST X-ray Photoelectron Spectroscopy Database, NIST Standard Reference Database, US Department of Commerce, Gaithersburg, MD (1997).
29 Kim, Y. T. & Bard, A. J. Imaging and etching of self-assembled n-octadecanethiol layers on gold with the scanning tunneling microscope. *Langmuir* **8,** 1096–1102 (1992).
30 Kitagawa, K., Morita, T., Kawasaki, M. & Kimura, S. Electric properties of self-assembled monolayers of helical peptides by scanning tunneling spectroscopy. *J. Polym. Sci. A Polym. Chem.* **41,** 3493–3500 (2003).
31 Kitagawa, K., Morita, T. & Kimura, S. Observation of single helical peptide molecule incorporated into alkanethiol self-assembled monolayer on gold by scanning tunneling microscopy. *J. Phys. Chem. B* **108,** 15090–15095 (2004).
32 Bourg, M., Badia, A. & Lennox, R. B. Gold-sulfur bonding in 2D and 3D self-assembled monolayers: XPS characterization. *J. Phys. Chem. B* **104,** 6562–6567 (2000).
33 McDermott, C. A., McDermott, M. T., Green, J. & Porter, M. D. Structural origins of the surface depressions at alkanethiolate monolayers on Au(111): a scanning tunneling and atomic force investigation. *J. Phys. Chem.* **99,** 13257–13267 (1995).
34 Dubois, L. H., Zegarski, B. R. & Nuzzo, R. G. Molecular ordering of organosulfur compounds on Au(111) and Au(100): Adsorption from solution and in ultrahigh vacuum. *J. Chem. Phys.* **98,** 678–688 (1993).
35 Poirier, G. E., Tarlov, M. J. & Rushmeier, H. E. Two-dimensional liquid phase and the px.sqroot.3 phase of alkanethiol self-assembled monolayers on Au(111). *Langmuir* **10,** 3383–3386 (1994).
36 Camillone, N. III, Eisenberger, P., Leung, T. Y. B., Schwartz, P., Poirier, G. E., Scoles, G. & Tarlov, M. J. New monolayer phases of n-alkanethiols self-assembled on Au(111): Preparation, surface characterization and imaging. *J. Chem. Phys.* **101,** 11031–11036 (1994).
37 Camillone, N. III Diffusion-limited thiol adsorption on the gold (111) surface. *Langmuir* **20,** 1199–1206 (2004).
38 Hayashi, T., Kodoma, C. & Nozoye, H. Structural evolution of dibutyldisulfide adsorbed on Au(111). *Appl. Surf. Sci.* **169-170,** 100–103 (2001).
39 Yamada, R. & Uosaki, K. *In situ,* real time monitoring of the self-assembly process of decanethiol on Au(111) in liquid phase. A scanning tunnelling microscopy investigation. *Langmuir* **13,** 5218–5221 (1997).
40 Pace, G., Venanzi, M., Castrucci, P., Scarselli, M., De Crescenzi, M., Palleschi, A., Stella, L., Formaggio, F., Toniolo, C. & Marletta, G. Static and dynamic features of a helical hexapeptide chemisorbed on a gold surface. *Mater. Sci. Eng. C* **26,** 918–923 (2006).
41 Poirier, G. E. & Tarlov, M. J. Molecular ordering and gold migration observed in butanethiol self-assembled monolayers using scanning tunnelling microscopy. *J. Phys. Chem.* **99,** 10966 (1995).
42 Stranick, S. J., Parick, A. N., Allara, D. L. & Weiss, P. S. A new mechanism for surface diffusion: motion of a substrate-adsorbate complex. *J. Phys. Chem.* **98,** 11136–11142 (1994).
43 Esplandiu, M. J. & Hagenström, H. Functionalized self-assembled monolayers and their influence on silver electrodeposition. *Solid State Ion* **150,** 39–52 (2002).
44 Antonello, S., Formaggio, F., Moretto, A., Toniolo, C. & Maran, F. Anomalous distance dependence of Electron Transfer across peptide bridges. *J. Am. Chem. Soc.* **125,** 2874–2875 (2003).
45 Xiao, X., Xu, B. & Tao, N. Conductance titration of single peptide molecules. *J. Am. Chem. Soc.* **126,** 5370–5371 (2004).
46 Long, Y. T., Abu-Irhayem, E. & Kraatz, H. B. Peptide electron transfer: more questions than answers. *Chem. Eur. J.* **11,** 5186–5194 (2005).
47 Morita, T., Kimura, S., Kobayashi, S. & Imanishi, Y. Photocurrent generation under a large dipole moment formed by self-assembled monolayers of helical peptides having an N-ethylcarbazolyl group. *J. Am. Chem. Soc.* **122,** 2850–2859 (2000).
48 Gatto, E., Stella, L., Formaggio, F., Toniolo, C., Lorenzelli, L. & Venanzi, M. Electroconductive and photocurrent generation properties of self-assembled monolayers formed by functionalized, conformationally-constrained peptides on gold electrodes. *J. Pept. Sci.* **14,** 184–191 (2008).
49 Toniolo, C., Crisma, M. & Formaggio, F. TOAC, a nitroxide spin-labeled, achiral C^{α}-tetrasubstituted α-amino acid, is an excellent tool in materials science and biochemistry. *Biopolym. Pept. Sci.* **47,** 125–158 (1998).
50 Hanson, P., Martinez, G., Millhauser, G., Formaggio, F., Crisma, M., Toniolo, C. & Vita, C. Distinguishing helix conformations in alanine-rich peptides using unnatural amino acid TOAC and electron spin resonance. *J. Am. Chem. Soc.* **118,** 271–272 (1996).
51 Milov, A. D., Tavetkov, Y. D., Formaggio, F., Crisma, M., Toniolo, C. & Rapp, J. The secondary structure of a membrane modifying peptide in a supramolecular assembly studied by PELDOR and CW-ESR spectroscopies. *J. Am. Chem. Soc.* **123,** 3784–3789 (2001).
52 Pispisa, B., Palleschi, A., Stella, L., Venanzi, M. & Toniolo, C. A nitroxide derivative as a probe for conformational studies of short linear peptides in solution. Spectroscopic and molecular mechanics investigations. *J. Phys. Chem. B* **102,** 7890–7898 (1998).
53 Venanzi, M., Gatto, E., Bocchinfuso, G., Palleschi, A., Stella, L., Baldini, C., Formaggio, F. & Toniolo, C. Peptide folding dynamics: a time-resolved study from the nanosecond to the microsecond time regime. *J. Phys. Chem. B* **110,** 22834–22841 (2006).
54 Wen, X., Linton, R. W., Formaggio, F., Toniolo, C. & Samulski, E. T. Self-assembled monolayers of hexapeptides on gold: surface characterization and orientation distribution analysis. *J. Phys. Chem. A* **108,** 9673–9681 (2004).
55 Brett, C. M. A. Electrochemistry. *Principles, Methods and Applications* (Oxford University Press, Oxford, 1993).
56 Watanabe, J., Morita, T. & Kimura, S. Effect of dipole moment, linkers, and chromophores at side chains on long-range electron transfer through helical peptides. *J. Phys. Chem. B* **109,** 14416–14425 (2005).
57 Fujita, K., Bunjes, N., Nakajima, K., Hara, M., Sasabe, H. & Knoll, W. Macrodipole interactions of helical peptides in a self-assembled monolayer on gold substrates. *Langmuir* **14,** 6167–6172 (1998).
58 Finklea, H. A. & Hanshew, D. D. Electron-transfer kinetics in organized thiol monolayer with attached pentaammine(pyridine)ruthenium redox centers. *J. Am. Chem. Soc.* **114,** 3173–3181 (1992).
59 Sek, S., Tolak, A., Misicka, A., Palys, B. & Bilewicz, R. Asymmetry of electron transmission through monolayers of helical polyalanine adsorbed on gold surfaces. *J. Phys. Chem. B* **109,** 18433–18438 (2005).
60 Gatto, E., Porchetta, A., Stella, L., Guryanov, I., Formaggio, F., Toniolo, C., Kaptein, B., Broxterman, Q. B. & Venanzi, M. Conformational effects on the electron transfer efficiency in peptide foldamers based on α,α-disubstituted glycyl residues. *Chem. Biodiv.* **5,** 1263–1278 (2008).
61 Cordes, M., Köttgen, A., Jasper, C., Jacques, O., Boudebous, H. & Giese, B. Influence of amino acid side-chains on long-distance Electron Transfer in peptides: Electron Hopping via 'stepping stones'. *Angew Chem.* **47,** 3461–3463 (2008).
62 Gray, H. B. & Winkler, J. R. Electron Transfer through proteins. *Q. Rev. Biophys.* **36,** 341–372 (2003).
63 Gray, H. B. & Winkler, J. R. Long-range Electron Transfer. *Proc. Natl Acad. Sci. USA* **102,** 3534–3539 (2005).
64 Yanagisawa, K., Morita, T. & Kimura, S. Efficient photocurrent generation by self-assembled monolayers composed of 3_{10}-helical peptides carrying linearly spaced Naphthyl groups at the side chains. *J. Am. Chem. Soc.* **126,** 12780–12781 (2004).
65 Yasutomi, S., Morita, T. & Kimura, S. pH-controlled switching of photocurrent detection by self-assembled monolayer of helical peptides. *J. Am. Chem. Soc.* **127,** 14564–14565 (2005).
66 Gatto, E., Venanzi, M., Palleschi, A., Stella, L., Pispisa, B., Lorenzelli, L., Toniolo, C., Formaggio, F. & Marletta, G. Self-assembled peptide monolayers on interdigitated gold microelectrodes. *Mater. Sci. Eng. C* **27,** 1309–1312 (2007).
67 Khazraji, T., Hotchandani, S., Das, S. & Kamat, P. V. Controlling dye (Merocyanine-540) aggregation on nanostructured TiO_2 films. An organized assembly approach for enhancing the efficiency of photosensitization. *J. Phys. Chem. B* **103,** 4693–4700 (1999).
68 Gatto, E., Stella, L., Baldini, C., Toniolo, C., Formaggio, F. & Venanzi, M. Photocurrent generation in peptide-based self-assembled monolayers on gold electrodes. *Superlatt. Microstruct.* **46,** 34–39 (2009).
69 Gatto, E., Caruso, M., Porchetta, A., Toniolo, C., Formaggio, F., Crisma, M. & Venanzi, M. Photocurrent generation through peptide-based self-assembled monolayers on a gold surface: antenna and junction effects. *J. Pept. Sci.* **17,** 124–131 (2011).
70 Wain, A. J., Do, H. N. L., Mandal, H. S., Kraatz, H. B. & Zhou, F. Influence of molecular dipole moment on the redox-induced reorganization of α-helical peptide self-assembled monolayers. An electrochemical SPR investigation. *J. Phys. Chem. C* **112,** 14513–14519 (2008).
71 Mandal, H. S. & Kraatz, H. B. Electron transfer across α-helical peptides: Potential influence of molecular dynamics. *Chem. Phys.* **326,** 246–251 (2006).
72 Kimura, S. Molecular dipole engineering: new aspects of molecular dipoles in molecular architecture and their functions. *Org. Biomol. Chem.* **6,** 1143–1148 (2008).
73 Gatto, E., Porchetta, A., Scarselli, M., De Crescenzi, M., Formaggio, F., Toniolo, C. & Venanzi, M. Playing with peptides: How to build a supramolecular peptide nanostructure by exploiting helix*( )helix macrodipole interactions. *Langmuir* **28,** 2817–2826 (2012).
74 Winnik, F. M. Photophysics of preassociated pyrenes in aqueous polymer solutions and in other organized media. *Chem. Rev.* **93,** 587–614 (1993).
75 Mandal, H. S., Burgess, I. J. & Kraatz, H. B. Investigation of laser induced photocurrent generation experiments. *Chem. Comm.* 4802–4804 (2006).
76 McCreery, R. L. Molecular electronic junctions. *Chem. Mater.* **16,** 4477–4496 (2004).

Mariano Venanzi, received his PhD in 1988 from the University of Rome 'La Sapienza' (Italy). He was visiting scientist at the University of Newcastle, the Max Planck Institut in Göttingen and the University of Melbourne. Since 1998 he is Associate Professor of Physical Chemistry at the Faculty of Sciences of the University of Rome Tor Vergata (UTV). His research interests focus on the spectroscopy of biomolecules for structural and photophysical studies, and on the development of peptide-based materials and the integration of biomolecules on hybrid devices. He is author of more than 160 publications on peer reviewed journals. He is member of the American Chemical Society, the European Peptide Society, the European Materials Research Society and in the Board of the Italian Chemical Society. Since 2007 he is the Chairman of the School of Chemistry at the Faculty of Sciences of UTV.

Emanuela Gatto was born in Rome, Italy, in 1978. She received her master degree cum laude in 2003 and her Doctoral degree of Chemistry in 2007, at the University of Rome Tor Vergata, under the supervision of prof. Mariano Venanzi. The Italian Chemical Society awarded her thesis "Conformationally constrained peptides as new nanomaterials for electrons and energy transfer" with the National Semeraro prize, as the best Ph.D. thesis in the Physical Chemistry field. In 2007 she has been a Marie Curie fellowship at the Division of Applied Physics of the University of Linkoping, Sweden. Since September 2007 she is working at the Department of Chemistry of the University of Rome Tor Vergata, where she is now Assistant Professor of Physical Chemistry. Her research activity is focused on the study of the secondary structure, electron and energy transfer processes of peptides, studied by a combination of spectroscopic and electrochemical techniques. Recently, a major interest has been related to electron transfer process in molecular systems immobilized on surfaces. Emanuela Gatto is author or co-author of 32 papers, all published on international and prestigious peer reviewed journals, of 14 publications on books and of several oral communications to national and international conferences.